Volume 16 | Number 9 | 7 May 2016 | Pages 1535–1710

Lab on a Chip

Miniaturisation for chemistry, physics, biology, materials science and bioengineering

www.rsc.org/loc

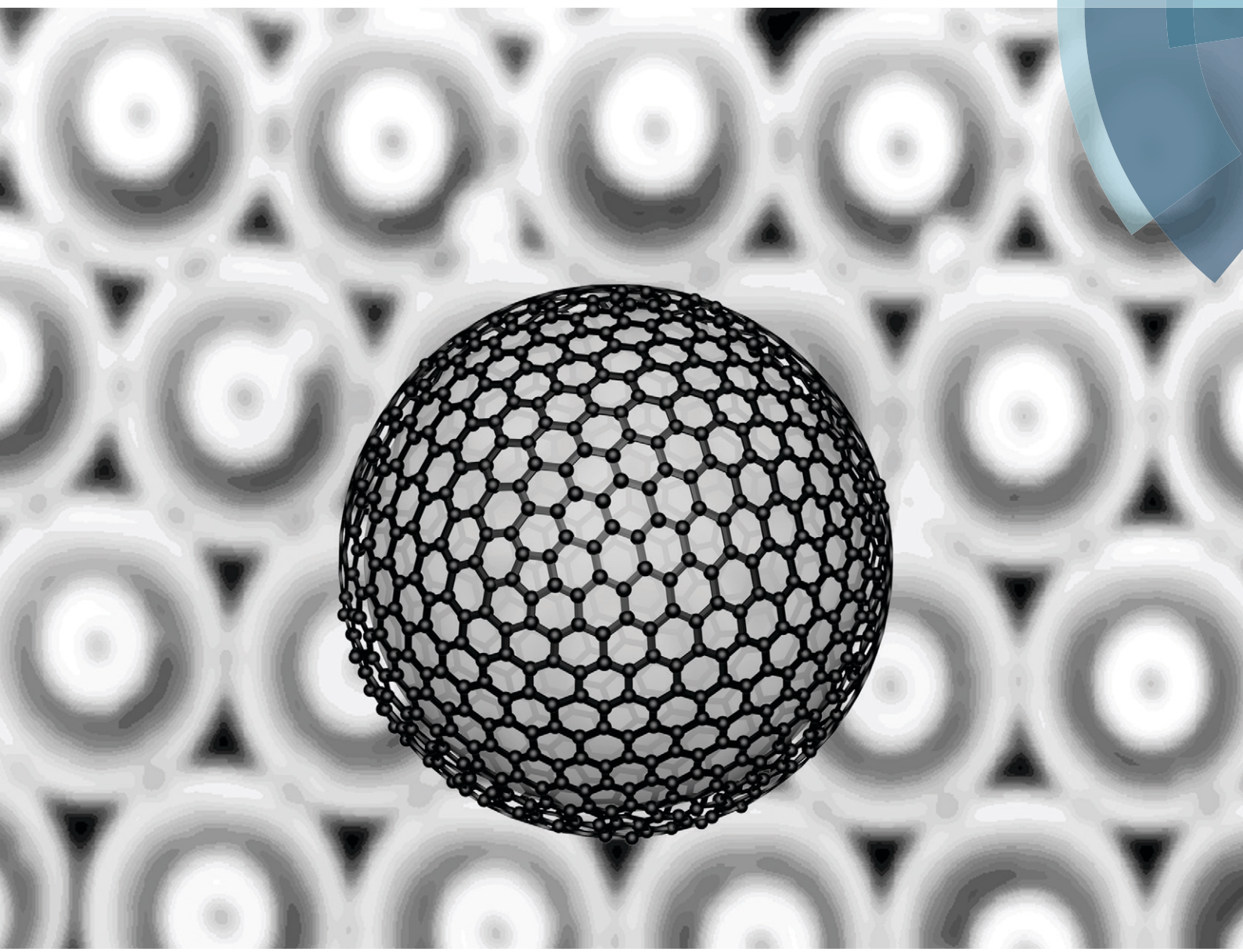

ISSN 1473-0197

ROYAL SOCIETY OF CHEMISTRY

PAPER
Jiandi Wan *et al.*
Stabilization of carbon dioxide (CO_2) bubbles in micrometer-diameter aqueous droplets and the formation of hollow microparticles

175 YEARS

Lab on a Chip

PAPER

View Article Online
View Journal | View Issue

Cite this: *Lab Chip*, 2016, **16**, 1587

Stabilization of carbon dioxide (CO_2) bubbles in micrometer-diameter aqueous droplets and the formation of hollow microparticles†

Tianyi Lu,[a] Rong Fan,[a] Luis F. Delgadillo[b] and Jiandi Wan*[a]

Received 22nd February 2016,
Accepted 16th March 2016

DOI: 10.1039/c6lc00242k

www.rsc.org/loc

We report an approach to stabilize carbon dioxide (CO_2) gas bubbles encapsulated in micrometer-diameter aqueous drops when water in the aqueous drops is evaporated. CO_2-in-water-in-oil double emulsion drops are generated using microfluidic approaches and evaporation is conducted in the presence of sodium dodecyl sulfate (SDS), poly(vinyl alcohol) (PVA) and/or graphene oxide (GO) particles dispersed in the aqueous phase of the double emulsion drops. We examine the roles of the bubble-to-drop size ratio, PVA and GO concentration in the stabilization of CO_2 bubbles upon water evaporation and show that thin-shell particles with encapsulated CO_2 bubbles can be obtained under optimized conditions. The developed approach offers a new strategy to study CO_2 dissolution and stability on the microscale and the synthesis of novel gas-core microparticles.

Introduction

Manipulation of the dissolution of carbon dioxide (CO_2) gas and the stability of CO_2 bubbles on the micrometer scale is of fundamental importance for many processes. Examples include micro-methanol fuel cells,[1,2] CO_2 sequestration in porous media,[3,4] gas exchange in the respiratory system,[5] carbon balance in oceans,[6] CO_2 enhanced oil recovery,[7,8] synthesis of functional microparticles[9–12] and chemical reactions involving CO_2.[13–15] Recent advances in microfluidics have achieved significant progress in the precise generation and manipulation of microbubbles and emulsion drops,[16–20] and thus have been utilized to study the dynamics of CO_2 dissolution and the formation of CO_2 bubble-based functional microparticles. The majority of microfluidic approaches for the study of CO_2 dissolution focus on segmented microflows in long serpentine microchannels, in which liquid plugs are separated by CO_2 gas bubbles.[21–24] The CO_2 bubbles usually have an initial diameter larger than the width of the microfluidic channel and come into contact with the solid wall *via* a thin layer of fluid. Although the kinetics of CO_2 dissolution can be derived by measuring the time-dependent size shrinkage of CO_2, the segmented flows of CO_2 bubbles affect gas absorption at the gas–liquid interfaces due to the recirculation flow in liquid plugs[25] and thus introduce additional complex factors to the dissolution process of CO_2, not to mention potential wetting problems between the bubbles and the channel wall. We have demonstrated the dissolution of CO_2 bubbles with an initial diameter smaller than the width of the channels and found that the dissolution of CO_2 bubbles goes through a rapid dissolution regime followed by an apparent equilibrium.[26] The observations are explained quantitatively by a multicomponent dissolution model that includes the effect of surface tension and the liquid pressure drop along the channel. In addition, by taking advantage of the acid–base equilibria during dissolution of CO_2 bubbles, microfluidic approaches have been developed to produce small CO_2 bubbles (<10 μm).[9] Most importantly, the increased acidity near CO_2 bubbles due to CO_2 dissolution in microchannels triggers the deposition of particles and/or polymers at the bubble–liquid interface, leading to significantly increased stability of CO_2 bubbles and the formation of microparticles with encapsulated CO_2 bubbles.[10–12] These particles have shown potential applications as drug delivery vehicles and ultrasound contrast agents.

While various microfluidic approaches have been developed to explore the dissolution and stabilization of CO_2 bubbles on the micrometer scale, less is known about the stability of CO_2 bubbles encapsulated in micrometer-diameter aqueous droplets.[27] Here, we developed a microfluidic approach to generate CO_2-in-water-in-oil double emulsions and investigated the stability of encapsulated CO_2 bubbles. In particular, we showed that, upon the

[a] *Microsystems Engineering, Rochester Institute of Technology, Rochester, New York, USA. E-mail: jdween@rit.edu*
[b] *Department of Biomedical Engineering, University of Rochester, Rochester, New York, USA*

† Electronic supplementary information (ESI) available: Calculations of CO_2 dissolution, microscopy image of CO_2-in-water-in-oil drops, change in the drop size and CO_2 bubble size with evaporation, change in percentages of CO_2-containing drops with evaporation, and typical force–distance curve of hollow particles. See DOI: 10.1039/c6lc00242k

removal of water from the aqueous phase of the drops *via* evaporation, the stability of CO_2 bubbles increased significantly in the presence of poly(vinyl alcohol) (PVA) and graphene oxide (GO) particles, and thin-shell particles with encapsulated CO_2 bubbles were formed. The present study thus demonstrates a new approach to stabilize CO_2 bubbles in confined micrometer-diameter droplets and the formation of CO_2-encapsulated microparticles, which we believe is of interest in many applications including the synthesis of CO_2-based functional microparticles and thin-shell particles, CO_2 storage, and the design of multiphase micro-reactors.

Experimental

Materials

CO_2 gas (99.97%) was ordered from Airgas. Poly(vinyl alcohol) (PVA, Mw 13 000–23 000, 87–89% hydrolysed) and sodium dodecyl sulfate (SDS) were purchased from Sigma-Aldrich and used as surfactants in the aqueous phase. Graphene oxide (GO) was ordered from Graphene Supermarket as dry platelets. Silicone oil (PDMS, polydimethylsiloxane, 20 cSt) was ordered from Sigma-Aldrich and used as the continuous oil phase. Dow Corning 749 fluid that contains 50 vol% high molecular weight resin and 50 vol% cyclopentasiloxane was ordered from Dow Corning and used as the surfactant in the PDMS oil phase.

Preparation of GO suspensions

A GO stock suspension with a particle concentration of 6 mg mL^{-1} was prepared by dispersing 30 mg of graphene oxide (GO) particles in 5 mL of DI water whose pH was pre-adjusted to 12 using a NaOH solution (1 M). The stock GO suspension was then sonicated using an ultrasonic cleaner (VWR Symphony Ultrasonic Cleaner) with a frequency of 35 kHz for half an hour. The particle size of GO in the suspension is approximately 10 to 25 μm examined under a microscope. GO suspensions of 0.5 mg ml^{-1}, 1.0 mg ml^{-1}, or 3.0 mg ml^{-1} were prepared by diluting the stock GO suspension accordingly.

Preparation of PVA solutions

Aqueous 10 wt% PVA solution was prepared as a stock solution by adding 20 g of PVA to 180 g of DI water. The PVA solution, under continuous stirring, was heated at 90 °C overnight to ensure complete dissolution of PVA. PVA solutions of 4 wt%, 5 wt%, or 6 wt% were prepared by diluting the stock solution accordingly. 5 wt% PVA solution with a varied GO concentration was prepared by adding 1 ml of GO stock solution and 5 mL of DI water (0.5 mg mL^{-1} GO), 2 ml of GO stock solution and 4 mL of DI water (1 mg mL^{-1} GO), or 6 ml of GO stock solution (3 mg mL^{-1} GO) to a 6 ml PVA stock solution.

Fabrication of glass capillary microfluidic devices

Microfluidic glass capillary devices, as shown in Fig. 1A, were fabricated based on established protocols.[28] Briefly, two cylindrical glass capillaries (standard glass capillaries 1/0.58 OD/ID mm, World Precision Instruments) with the same inner diameter of 0.58 mm were tapered using a pipette puller to obtain inner diameters of 160 μm and 320 μm, which were used as the injection (gas phase) and collection capillaries, respectively. The tapered part of the injection capillary was treated with *n*-octyltriethoxysilane. The injection and collection capillaries were fitted into a square capillary that has an inner diameter of 1.05 mm.

Generation of double-emulsion

Innermost gas phase CO_2 flows into the injection capillary with pressure P_G (P_G = 1.3 psi). The aqueous phase and the continuous oil phase flow through the two sides of the square capillary with flow rates of Q_w = 8–21.2 ml h^{-1} and Q_o = 18.2–29.5 ml h^{-1}, respectively. As CO_2 arrived at the tip of the tapered capillary, CO_2 was encapsulated into aqueous drops and then the gas phase and aqueous phase were emulsified into the continuous oil phase in a dripping regime. Syringe pumps (New Era Pump Systems) were used to adjust the liquid flow rates. CO_2 injection pressure was controlled by a pressure regulator (OMEGA, PRG200). A high-speed

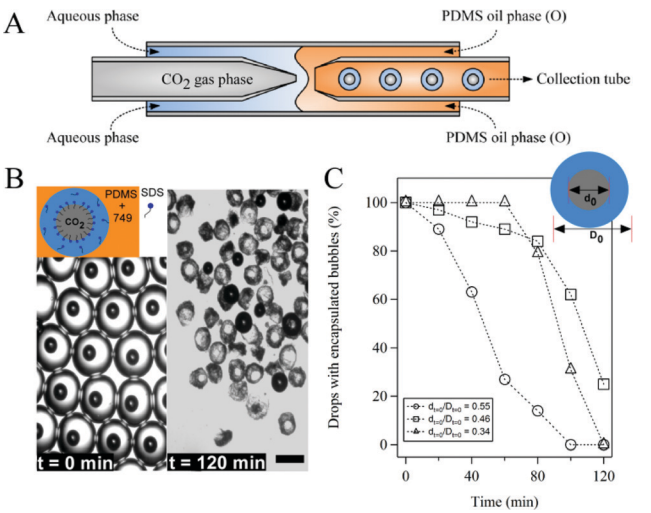

Fig. 1 Microfluidic generation of CO_2-in-water-in-oil double emulsion drops and the stability of encapsulated CO_2 microbubbles upon water evaporation. (A) Schematic of the microfluidic setup for the generation of CO_2-in-water-in-oil drops. Aqueous phase: DI water with 2.5 wt% SDS; oil phase: PDMS oil with 2 wt% 749. (B) Typical images of the drops with encapsulated CO_2 microbubbles before and after evaporation at room temperature. t = 0 min is defined as the time when the drops are collected outside the microfluidic device. Scale bar: 200 μm. Inset: schematic of a CO_2-in-water-in-oil drop in the presence of SDS. (C) The change in percentages of CO_2-containing drops with evaporation time at different initial bubble-to-drop diameter ratios. $d_{t=0}$ and $D_{t=0}$ are the diameters of the bubble and drop (shown in inset), respectively, when they were collected outside the microfluidic device.

camera (Phantom M120) coupled to an optical microscope (IN480T-FL, Amscope) was used to monitor the generation process of CO_2-in-water-in-oil double emulsions. The continuous oil phase was PDMS oil with 2 wt% 749 fluid. The aqueous phase was DI water with 1–2.5 wt% SDS. To examine the effect of PVA and GO on the stability of encapsulated CO_2 bubbles upon evaporation, PVA and GO suspensions with various concentrations were added to the aqueous phase.

Evaporation of emulsion drops

CO_2-in-water-in-oil double emulsion droplets in a continuous oil phase (~8 μL) were collected on a glass slide and the aqueous phase of the drops was allowed to evaporate at room temperature for 120 min. To monitor the evaporation process, a microscopy image of the double drops was recorded every 10 min using the high-speed camera (Phantom M120). ImageJ was used to analyze the size of the bubbles and drops.

Scanning electron microscopy

Particles generated from double emulsion droplets upon evaporation were washed with isopropyl alcohol, and then dried and coated with a thin layer of gold. The particles were characterized by SEM (Amray 1830) at an accelerating voltage of 20 kV.

Atomic force microscopy

Contact mode measurements were performed with an MFP-3D atomic force microscope (Asylum Research, Santa Barbara, CA). Silicon nitride AFM cantilevers (Asylum Research, Santa Barbara, CA) with spring constants in the range of 30 pN nm^{-1} were used to indent into a single hollow particle. To prevent the spheres from shifting during indentation, the particles were adhered to a glass slide with an ultraviolet curing optical adhesive (Norland Products, Cranbury, NJ). The cantilever was positioned over the top of a single particle and indented with a loading rate of 2 μm s^{-1} and a maximum indentation force of 5 nN. Force and distance curves were calculated by multiplying the cantilever deflection with the spring constant for the force curves and by subtracting the cantilever deflection from the height position for the distance curves. Results were obtained based on measurements from seven different particles and at different measuring positions.

Results and discussion

Stability of encapsulated CO_2 bubbles in the presence of SDS

We utilized a glass capillary microfluidic device to generate CO_2-in-water-in-oil double emulsion drops and investigated the stability of CO_2 microbubbles upon evaporating the aqueous phase (Fig. 1A). In particular, DI water with SDS and PDMS oil with 749 fluid as surfactants were used as the aqueous and continuous oil phases, respectively. After CO_2-in-water-in-oil double emulsion drops were generated, the size of CO_2 bubbles decreased quickly inside the microfluidic channel and reached a constant size after being collected outside the microfluidic device (Fig. S1†). The stabilization of the size of CO_2 bubbles in drops was likely due to saturation of the aqueous drops with dissolved CO_2. Indeed, the actual concentration of dissolved CO_2 in our experiments was close to the estimated concentration of dissolved CO_2 based on Henry's law (Table S1†).

We then studied the stability of CO_2 bubbles when the aqueous phase was allowed to evaporate for 120 min at room temperature. Fig. 1B shows the typical images of drops before and after evaporation. Evidently, the majority of CO_2 bubbles disappeared after water was removed and hollow particles were formed. The shell of the particle was presumably composed of SDS and the non-volatile, polymeric components of 749 fluid. When we changed the size of bubbles (d_0) and drops (D_0) and studied the effect of size ratio (d_0/D_0) on the stability of CO_2 bubbles, the percentage of drops with encapsulated bubbles decreased with time for all three size ratios (d_0/D_0 = 0.55, 0.46 and 0.34) (Fig. 1C). Particularly, the percentage of drops with the highest size ratio (d_0/D_0 = 0.55) decreased the fastest and the drops with a mid-range size ratio (*e.g.*, d_0/D_0 = 0.46) had slightly better performance than the drops with the two other size ratios at the end of evaporation.

The observed phenomena might be due to an interfacial instability at the early stage of evaporation and the effect of a solid shell at the late stage of evaporation. Because the size of drops became smaller as the aqueous phase evaporated (Fig. S2†), the surface area of the drops decreased. As a result, the concentration of SDS and surfactant 749 at the aqueous–oil interface increased. This non-equilibrium absorbed excess of surfactants can trigger an interfacial instability and lead to explosion of drops.[29] When the thickness of the aqueous layer between bubbles and drops was small (the bubble-to-drop size ratio was large, *e.g.*, d_0/D_0 = 0.55), encapsulated bubbles encountered this instability at the early time of evaporation and burst, resulting in a quickly decreased percentage of drops with encapsulated bubbles, as observed in Fig. 1C. On the other hand, when the thickness of the aqueous layer between bubbles and drops was large (the bubble-to-drop size ratio was small, *e.g.*, d_0/D_0 = 0.34), the bubbles were relatively stable at the early time of evaporation (Fig. 1C). However, when a sol–gel transition of the aqueous layer occurred in the middle of evaporation, the viscous liquid in the aqueous layer transformed into a solid shell with a relatively large thickness due to the small d_0/D_0. Although the thick elastic shell of a capsule had a large threshold buckling pressure and was stable against shell deformation during water evaporation,[30,31] the shell would also exert large stresses to the encapsulated bubbles if the size of the bubbles kept increasing, which would lead to bubble instability. Indeed, increased bubble size upon evaporation was observed (Fig. S3†), presumably due to the diffusion of gases (*e.g.*, O_2 or N_2) from the surrounding environment.[26,27] As a result, the stability of bubbles with a small d_0/D_0 at the later stage of evaporation decreased quickly (Fig. 1C). The relatively high percentage of

drops with stable encapsulated bubbles for a mid-range bubble-to-drop size ratio (*e.g.*, d_0/D_0 = 0.46) (Fig. 1C) was likely due to the minimized effect of interfacial instability at the early stage of evaporation and a relatively low buckling pressure of the shell at the later stage of evaporation.

Effect of poly(vinyl alcohol) (PVA) on the stability of CO_2 bubbles upon evaporation

Because PVA is an effective emulsifier and can stabilize water–oil or gas–water interfaces and increase the viscosity of the aqueous phase,[28,32,33] we tested the effect of PVA on the stability of CO_2 bubbles upon evaporation. Particularly, we added 4 wt%, 5 wt%, or 6 wt% PVA to the aqueous drops in the presence of SDS. Fig. 2A shows the typical images of drops with 4 wt% PVA upon evaporation. The percentage of drops with encapsulated bubbles increased significantly after evaporation (Fig. 2B) compared to that of drops in the absence of PVA (Fig. 1B). This observation held true for all three different bubble-to-drop size ratios and followed the same pattern observed in Fig. 1C where the percentage of drops with a mid-range size ratio was the highest. In addition, the percentage of drops with encapsulated bubbles increased with the increase of PVA concentration (Fig. 2C & D) and reached the highest percentage of 96% when 6 wt% PVA was used for d_0/D_0 = 0.36 (Fig. 2D). Because the bulk viscosity of drops increased due to the addition of PVA, the increased interfacial area of drops upon water evaporation could be presented as folding or deformation of the interface instead of explosion.[29] As a result, CO_2 bubbles in PVA-containing drops were expected to be more stable than those in PVA-free drops. Indeed, the deformation (or buckling) of the PVA-containing shell was clearly observed at t = 120 min (Fig. 2A).

Effect of graphene oxide (GO) on the stability of CO_2 bubbles upon evaporation

GO particles have been used as colloidal surfactants to stabilize interfaces including CO_2 gas bubbles in aqueous phases,[34,35] and play roles in controlling gas diffusion.[36,37] We thus hypothesize that adding GO will further stabilize CO_2 bubbles in drops upon evaporation. To test this hypothesis, we added GO at a concentration of 1 mg ml^{-1} to the aqueous phase in the presence of SDS and 5 wt% PVA. Fig. 3A shows the typical microscopy images of CO_2-in-water-in-oil emulsion drops before and after water evaporation in the presence of GO. 94% of drops still contained CO_2 bubbles after 120 min of evaporation. In comparison, the highest percentage of drops with encapsulated CO_2 bubbles was 81% when GO was absent in the aqueous drops (Fig. 2C). Remarkably, hollow particles with a relatively thin shell around CO_2 bubbles were formed and some of the particles exhibited a hexagonal shape (Fig. 3A). The thickness of the shell was measured to be 23.4 ± 9.2 μm. This observation was completely absent when drops were evaporated without GO (Fig. 1B and 2A). Adding filler particles such as GO into polymer matrices can control the stress distribution in the polymer matrix, transfer applied stress from the matrix to the particle, and thus increase the strength of the polymer matrix.[38,39] As a result, the mechanical stress arising from the

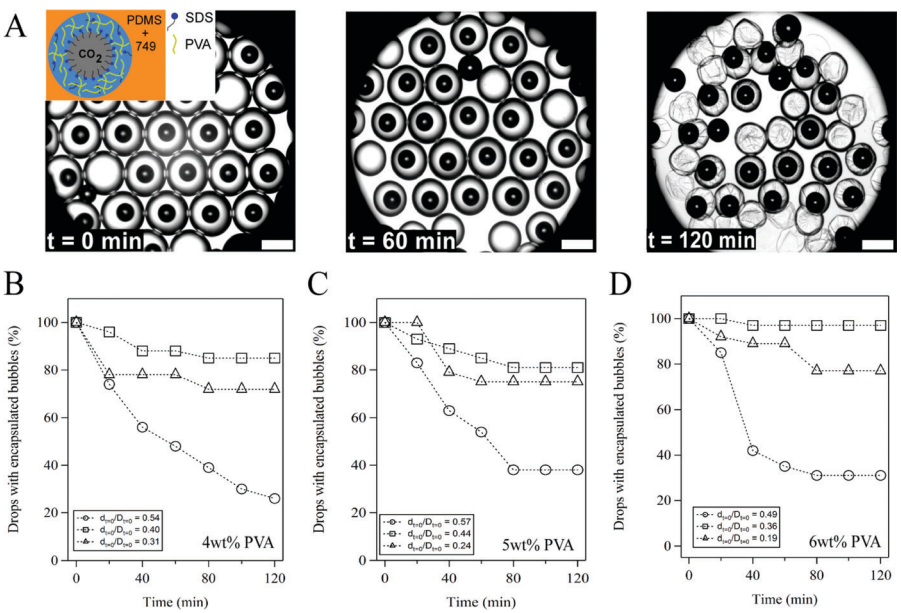

Fig. 2 Effect of poly(vinyl alcohol) (PVA) on the stability of CO_2 microbubbles upon water evaporation. (A) Images of drops with encapsulated CO_2 microbubbles at different times of evaporation. The aqueous phase contains 1 wt% SDS and 4 wt% PVA. The PDMS oil phase contains 2 wt% 749. $d_{t=0}/D_{t=0}$ = 0.4. Inset: schematic of a CO_2-in-water-in-oil drop in the presence of SDS and PVA. Scale bar: 400 μm. Change in percentages of CO_2-containing drops with evaporation time at different initial bubble-to-drop diameter ratios in the presence of (B) 4 wt%, (C) 5 wt% and (D) 6 wt% PVA.

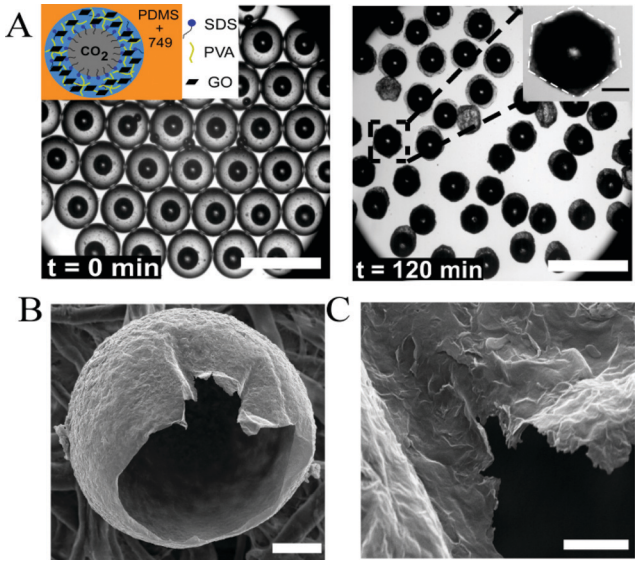

Fig. 3 Evaporation-induced formation of hollow particles in the presence of graphene oxide (GO). (A) Images of drops with encapsulated CO_2 microbubbles before and after evaporation at room temperature. The aqueous phase contains 1 wt% SDS, 5 wt% PVA and 1 mg ml^{-1} GO. The PDMS oil phase contains 2 wt% 749. Inset: schematic of a CO_2-in-water-in-oil drop in the presence of SDS, PVA and GO. Scale bar: 700 μm. Inset: microscopic image of a particle with hexagonal morphology. Scale bar: 100 μm. (B) SEM image of a single hollow particle. Scale bar: 50 μm. (C) High-magnification SEM image of the shell. Scale bar: 5 μm.

expansion of bubbles upon evaporation was likely distributed evenly on the PVA–GO composite, resulting in a shell with a relatively homogeneous thickness. Increased GO concentration such as 3 mg ml^{-1}, however, compromised the stability of encapsulated CO_2 bubbles (Fig. S4†), presumably due to the poor dispersion of GO at high concentrations.

We further characterized the particles using SEM (Fig. 3B and C) and found that the surface of the particles had layered structures and was relatively smooth (no significant deformation, for example). Because the elastic modulus of the shell determined by AFM was 2.85 ± 1.2 MPa (Fig. S5†), the threshold buckling pressure ($P_{buckling}$) could be estimated to be 97.9 kPa using the shell theory $P_{bucking} \cong \frac{2E}{\left(3\left(1-\nu^2\right)\right)^{1/2}}\left(h/R\right)^2$,[40] where E (= 2.85 ± 1.2 MPa) and ν (≈1/3) are the Young's modulus and Poisson's ratio of the shell, respectively; and h (= 23.4 ± 9.2 μm) and R (= 140 ± 6.8 μm) are the thickness and radius of the shell, respectively. Thus, a relatively large capillary pressure will be needed to deform the shell, which explained the observed smooth surface of the particles. Note that the calculated $P_{buckling}$ was close to a recently reported value of 95.8 kPa in a poly(DL-lactic-*co*-glycolic acid) (PLGA) shell with encapsulated CO_2 gas.[27]

To further identify the roles of GO in stabilizing encapsulated CO_2 bubbles, we did the same experiments in the absence of PVA. The results showed that, after evaporating the aqueous phase, the percentage of drops with encapsulated CO_2 bubbles was high (95–98%) and did not change significantly compared to that in the presence of PVA (Fig. 4A and B), suggesting that GO (along with SDS) can stabilize encapsulated CO_2 bubbles upon evaporation. We did, however, find that, in the absence of PVA, CO_2 bubbles started to extrude from the drops, and acorn-shaped particles with encapsulated CO_2 bubbles were formed at the later stage of evaporation (Fig. 4C and D). Because PVA acted as the polymer matrix in the PVA–GO composite shell, the absence of PVA significantly impaired the strength of the shell (or linkage between GO particles),[39] and consequently resulted in bubble extrusion when bubbles expanded upon evaporation. Similar acorn-shaped particles have been observed in phase separation-induced anisotropic polymeric particles where polymer–solvent (and polymer) interactions and interfacial energy play a key role.[41,42] In our case, it was also likely that the decreased interfacial tension between CO_2 and the oil phase in the presence of GO contributed to the formation of acorn-shaped particles.

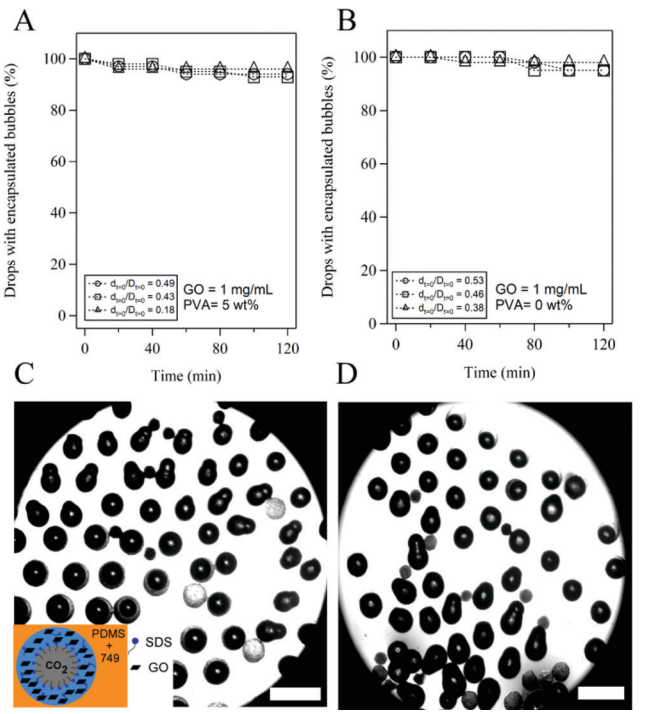

Fig. 4 Effect of graphene oxide (GO) on the stability of CO_2 microbubbles encapsulated in aqueous drops in the absence of PVA. (A) and (B) show, respectively, the change in percentages of CO_2-containing drops with evaporation time with and without PVA. (C) and (D) are, respectively, the microscopic images of drops with encapsulated CO_2 microbubbles after evaporation (t = 120 min) at $d_{t=0}/D_{t=0}$ = 0.53 and $d_{t=0}/D_{t=0}$ = 0.38. The aqueous phase contains 1 mg ml^{-1} GO and 2 wt% SDS. The PDMS oil phase contains 2 wt% 749. Inset: schematic of a CO_2-in-water-in-oil drop in the presence of SDS and GO. Scale bar: 500 μm.

Conclusions

In summary, we demonstrated a new approach to stabilize CO_2 bubbles confined in micrometer-diameter aqueous droplets and unveiled the roles of PVA and GO in the stabilization of encapsulated CO_2 bubbles upon water evaporation. In addition, by optimizing the bubble-to-drop size ratio, PVA and GO concentration, thin-shell microparticles with encapsulated CO_2 bubbles were observed. Although microfluidic approaches for the synthesis of gas-core particles have been demonstrated previously,[18,28,30] the evaporation-induced formation of particles using diffusive gases such as CO_2 as the gas core is less studied. Thus, the developed approach not only provides new insights into the stability of CO_2 bubbles but also paves a new way to produce gas-core particles, which are known to have many applications in a wide range of fields.

Acknowledgements

The authors gratefully acknowledge the support from the Rochester Institute of Technology for Jiandi Wan. Jiandi Wan also acknowledges the Donors of the American Chemical Society Petroleum Research Fund for partial support of this research.

Notes and references

1 D. D. Meng, T. Cubaud, C. M. Ho and C. J. Kim, *J. Microelectromech. Syst.*, 2007, **16**, 1403–1410.
2 P. Argyropoulos, K. Scott and W. M. Taama, *Electrochim. Acta*, 1999, **44**, 3575–3584.
3 G. Bhattacharjee, A. Kumar, T. Sakpal and R. Kumar, *ACS Sustainable Chem. Eng.*, 2015, **3**, 1205–1214.
4 M. Talebian, R. Al-Khoury and L. J. Sluys, *Adv. Water Resour.*, 2013, **59**, 238–255.
5 J. B. Grotberg, *Phys. Fluids*, 2011, **23**, 021301.
6 J. C. Orr, V. J. Fabry, O. Aumont, L. Bopp, S. C. Doney, R. A. Feely, A. Gnanadesikan, N. Gruber, A. Ishida and F. Joos, *Nature*, 2005, **437**, 681–686.
7 M. Nobakht, S. Moghadam and Y. Gu, *Energy Fuels*, 2007, **21**, 3469–3476.
8 J. F. M. Orr and J. J. Taber, *Science*, 1984, **224**, 563–569.
9 J. I. Park, Z. Nie, A. Kumachev and E. Kumacheva, *Soft Matter*, 2010, **6**, 630–634.
10 J. I. Park, E. Tumarkin and E. Kumacheva, *Macromol. Rapid Commun.*, 2010, **31**, 222–227.
11 J. I. Park, D. Jagadeesan, R. Williams, W. Oakden, S. Chung, G. J. Stanisz and E. Kumacheva, *ACS Nano*, 2010, **4**, 6579–6586.
12 J. I. Park, Z. Nie, A. Kumachev, A. I. Abdelrahman, B. P. Binks, H. A. Stone and E. Kumacheva, *Angew. Chem., Int. Ed.*, 2009, **48**, 5300–5304.
13 M. A. Dureen and D. W. Stephan, *J. Am. Chem. Soc.*, 2010, **132**, 13559–13568.
14 P. G. Jessop, D. J. Heldebrant, X. W. Li, C. A. Eckert and C. L. Liotta, *Nature*, 2005, **436**, 1102.
15 G. Lestari, M. Abolhasani, D. Bennett, P. Chase, A. Günther and E. Kumacheva, *J. Am. Chem. Soc.*, 2014, **136**, 11972–11979.
16 P. Garstecki, M. J. Fuerstman, H. A. Stone and G. M. Whitesides, *Lab Chip*, 2006, **6**, 437–446.
17 J. Wan and H. A. Stone, *Soft Matter*, 2010, **6**, 4677–4680.
18 J. Wan, A. Bick, M. Sullivan and H. A. Stone, *Adv. Mater.*, 2008, **20**, 3314–3318.
19 K. Khoshmanesh, A. Almansouri, H. Albloushi, P. Yi, R. Soffe and K. Kalantar-zadeh, *Sci. Rep.*, 2015, **5**, 9942.
20 M. Lee, E. Y. Lee, D. Lee and B. J. Park, *Soft Matter*, 2015, **11**, 2067–2079.
21 M. Abolhasan, M. Singh, E. Kumacheva and A. Gunther, *Lab Chip*, 2012, **12**, 1611–1618.
22 R. Sun and T. Cubaud, *Lab Chip*, 2011, **11**, 2924–2928.
23 T. Cubaud, M. Sauzade and R. Sun, *Biomicrofluidics*, 2012, **6**, 22002–220029.
24 S. G. Lefortier, P. J. Hamersma, A. Bardow and M. T. Kreutzer, *Lab Chip*, 2012, **12**, 3387–3391.
25 A. Günther, M. Jhunjhunwala, M. Thalmann, M. A. Schmidt and K. F. Jensen, *Langmuir*, 2005, **21**, 1547–1555.
26 S. Shim, J. Wan, S. Hilgenfeldt, P. D. Panchal and H. A. Stone, *Lab Chip*, 2014, **14**, 2428–2436.
27 M. H. Lee and D. Lee, *Soft Matter*, 2010, **6**, 4326–4330.
28 H. Chen, J. Li, J. Wan, D. A. Weitz and H. A. Stone, *Soft Matter*, 2013, **9**, 38–42.
29 S. Liu, R. Deng, W. Li and J. Zhu, *Adv. Funct. Mater.*, 2012, **22**, 1692–1697.
30 A. Abbaspourrad, W. J. Duncanson, N. Lebedeva, S. H. Kim, A. P. Zhushma, S. S. Datta, P. A. Dayton, S. S. Sheiko, M. Rubinstein and D. A. Weitz, *Langmuir*, 2013, **29**, 12352–12357.
31 N. Tsapis, E. R. Dufresne, S. S. Sinha, C. S. Riera, J. W. Hutchinson, L. Mahadevan and D. A. Weitz, *Phys. Rev. Lett.*, 2005, **94**, 018302.
32 K. Yuki, T. Sato, H. Maruyama, J. Yamauchi and T. Okaya, *Polym. Int.*, 1993, **30**, 513–517.
33 K. M. Rosenblatt and H. Bunjes, *Mol. Pharmaceutics*, 2009, **6**, 105–120.
34 J. Kim, L. J. Cote, F. Kim, W. Yuan, K. R. Shull and J. Huang, *J. Am. Chem. Soc.*, 2010, **132**, 8180–8186.
35 C. N. Yeh, K. Raidongia, J. Shao, Q. H. Yang and J. Huang, *Nat. Chem.*, 2014, **7**, 166–170.
36 H. W. Kim, H. W. Yoon, S. M. Yoon, B. M. Yoo, B. K. Ahn, Y. H. Cho, H. J. Shin, H. Yang, U. Paik, S. Kwon, J. Y. Choi and H. B. Park, *Science*, 2013, **342**, 91–95.
37 P. Tzeng, B. Stevens, I. Devlaming and J. C. Grunlan, *Langmuir*, 2015, **31**, 5919–5927.
38 S. I. Abdullah and M. N. M. Ansari, Mechanical properties of graphene oxide (GO)/epoxy composites, *HBRC Journal*, 2015, **11**, 151–156.
39 S. Fua, X. Feng, B. Lauke and Y. Mai, *Composites, Part B*, 2008, **39**, 933–961.
40 S. S. Datta, S. H. Kim, J. Paulose, A. Abbaspourrad, D. R. Nelson and D. A. Weitz, *Phys. Rev. Lett.*, 2012, **109**, 134302.
41 T. Kong, Z. Liu, Y. Song, L. Wang and H. C. Shum, *Soft Matter*, 2013, **9**, 9780–9784.
42 N. G. Min, B. Kim, T. Y. Lee, D. Kim, D. C. Lee and S. H. Kim, *Langmuir*, 2015, **31**, 937–943.

